Molecular lens applied to benzene and carbon disulfide molecular beams

Hoi Sung Chung, Bum Suk Zhao, Sung Hyup Lee, Sungu Hwang, Keunchang Cho, Sang-Hee Shim, Soon-Mi Lim, Wee Kyung Kang, and Doo Soo Chung

Citation: The Journal of Chemical Physics **114**, 8293 (2001); doi: 10.1063/1.1367380

View online: http://dx.doi.org/10.1063/1.1367380

View Table of Contents: http://scitation.aip.org/content/aip/journal/jcp/114/19?ver=pdfcov

Published by the AIP Publishing

Molecular lens applied to benzene and carbon disulfide molecular beams

Hoi Sung Chung, Bum Suk Zhao, Sung Hyup Lee, Sungu Hwang, Keunchang Cho, Sang-Hee Shim, and Soon-Mi Lim
School of Chemistry, Seoul National University, Seoul 151-747, Korea

Wee Kyung Kang
Department of Chemistry, Soongsil University, Seoul 156-743, Korea

Doo Soo Chung[a)]
School of Chemistry, Seoul National University, Seoul 151-747, Korea

(Received 30 October 2000; accepted 2 March 2001)

A molecular lens of the nonresonant dipole force formed by focusing a nanosecond IR laser pulse has been applied to benzene and CS_2 molecular beams. Using the velocity map imaging technique for molecular ray tracing, characteristic molecular lens parameters including the focal length (f), minimum beam width (W), and distance to the minimum beam width position (D) were determined. The laser intensity dependence of the observed lens parameters was in good agreement with theoretical predictions. W was independent of the laser peak intensity (I_0), whereas f and D varied linearly with $1/I_0$. The differences in lens parameters between the molecular species were well correlated with the polarizability per mass values of the molecules. A high chromatographic resolution of $Rs=0.84$ was achieved between the images of benzene molecular beams undeflected and deflected by the lens. The possibilities for a new type of chromatography are discussed. © *2001 American Institute of Physics.* [DOI: 10.1063/1.1367380]

I. INTRODUCTION

When a nonresonant laser beam is focused onto molecules, the interaction between the laser electric field and the induced molecular dipole moment can exert a mechanical force on the molecules proportional to the laser intensity gradient. This nonresonant dipole force has been successfully used to control neutral molecules. By focusing intense nanosecond Nd:YAG or CO_2 laser pulses, deflection of molecular beams of simple linear molecules such as I_2 and CS_2 was demonstrated.[1,2] Intense laser fields also have been used to control the molecular orientation. A theoretical description was given for the pendular motion of molecules about the axis of polarization of an intense laser field,[3] and this alignment effect of molecules was observed by Raman experiments on two intermolecular bonds of a naphthalene trimer.[4] Molecular alignment with the laser polarization was also observed using an ion imaging technique.[5–7] Analogous to an optical lens focusing a photon beam, a molecular lens focusing a molecular beam can be formed using the nonresonant dipole force. Many theoretical aspects of a molecular lens were discussed by Seideman[8,9] and experiments on a cylindrical molecular lens formed by focusing a nonresonant IR laser pulse were recently reported.[10]

In this paper we report on a molecular lens of the nonresonant dipole force which was applied to manipulate benzene and CS_2 molecular beams in detail. Ray tracing of the molecular lens was performed by applying a velocity map imaging technique[11] on the molecular ions produced by resonance-enhanced multiphoton ionization (REMPI) of deflected neutral molecules. The velocity map imaging technique, where ions of the same velocity are focused into a point on a 2D ion image detector regardless of their positions in the ionization region, provided dramatically enhanced resolution for a detailed investigation of molecular rays affected by the molecular lens. The characteristic molecular lens parameters were determined from the tracing and their dependence on the laser intensity was studied. In accordance with theoretical predictions, the focal length (f) and distance to the minimum beam width position (D) were inversely proportional to the laser intensity, and the minimum beam width (W) was independent of the laser intensity. A chromatographic resolution of 0.84 was achieved between the molecular ray deflected by the lens and the one unaffected by the lens. Analogous to the dispersion of an optical lens depending on the wavelength of photon beams, the deflection of molecular beams by a molecular lens depends on molecular properties such as the mass and polarizability.

In order to trap neutral molecules in space, all three Cartesian components of molecular motion should be reduced to zero by applying light forces three-dimensionally. In contrast, the separation of molecules can be achieved by a single directional force exerted differently on each molecular species. The separation of molecules using a light force, therefore, should be much easier than the trapping of molecules, at least in principle. We have confirmed the possibility of separation of molecules with the light force by observing that the lens parameters correlate well with the polarizability per mass ratios of the molecular species.

II. EXPERIMENT

A schematic diagram of the vacuum chamber is shown in Fig. 1. The x axis is the laser propagation direction, the y

a)Author to whom correspondence should be addressed. Tel: +82-2-880-8130; Fax: +82-2-877-3025; electronic mail: dschung@snu.ac.kr

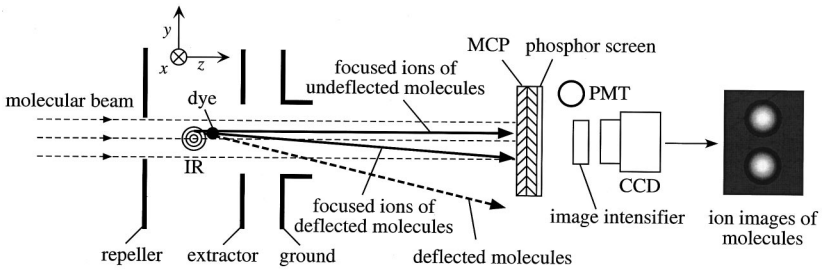

FIG. 1. Schematics of the setup: the inside of the chamber, electrodes, detectors, and the coordinate convention. The molecular beam propagates along the *z* axis and the laser beam along the *x* axis. Dipole force is exerted along the *y* axis. The neutral molecules deflected by the upper region of the molecular lens proceed downwards. After 34 ns, they are ionized by a dye laser pulse and focused onto a detector by the electrode system. The image of molecular ions on the phosphor screen is detected by PMT or intensified by an image intensifier for recording with a CCD camera.

axis the molecular beam deflection axis, and the *z* axis the direction of molecular beam. The vacuum system consists of two differentially pumped chambers, source and detection chambers, which are separated by a skimmer with a 0.51 mm diam hole. The source chamber, containing a pulsed valve (9-365-900 Solenoid Valve, Parker Instrumentation), is pumped by a 2400 l/s oil diffusion pump (VHS-6, Varian) with a rotary backing pump, yielding a pressure of 8.0×10^{-7} Torr. The detection chamber is a 200 mm cube with two 36 mm windows for laser beams on each side and a 570 mm TOF tube with a 2D-imaging detector at its end. The pressure inside the detection chamber is about 10^{-7} Torr, which is maintained by pumping with a 250 l/s turbomolecular pump (Turbo-V 250, Varian) and a rotary backing pump.

Pulsed supersonic molecular beams are formed by expanding 50 Torr benzene or CS_2 in 2 atm Ar through a 0.5 mm diam valve nozzle at a rate of 10 Hz with a 220 μs duration, which makes the source chamber pressure about 10^{-6} Torr. The molecular beam travels to the detection chamber through the 0.51 mm diam skimmer and a 0.6 mm diam pinhole along the *z* axis. The nozzle and pinhole determine the molecular beam size at the point of deflection. The estimated divergence of the molecular beam is $\pm0.5°$. The velocity of a molecular beam along the *z* axis is given by[12]

$$v_z=\left(\frac{2c_pT_0}{M}\right)^{1/2}, \tag{1}$$

where M is the number-averaged molecular weight of the gas mixture, c_P is the number-averaged molar heat capacity at constant pressure of the gas mixture, and $T_0=293$ K is the initial temperature. Benzene and CS_2 molecular beam velocities are 570 m/s and 560 m/s, respectively.

After propagating 85 mm from the nozzle, molecules are crossed by a 7 ns (FWHM) IR ($\lambda=1064$ nm) Nd:YAG laser pulse (Surelite II-10, Continuum) propagating along the *x* axis. The laser pulse is focused with an $f=175$ mm convex lens. The molecular beam is deflected by the nonresonant dipole force of a laser field whose energy and polarization are adjusted by a zero-order half-wave plate, a Glan-laser polarizer, and a quarter-wave plate. The energy of the circularly polarized laser pulse is adjusted in the range from 24 mJ to 64 mJ. The waist radius (ω_0) of the focused IR laser is about 14.5 μm. The peak intensity of the IR laser is varied up to 8.4×10^{11} W/cm^2, which scarcely ionizes the molecules.[13]

After a delay of 34 ns, the deflected molecular beam is crossed by a 5 ns (FWHM) dye laser (ND6000, Continuum) pulse ($\lambda=477.4$ nm for benzene, 483.0 nm for CS_2) which is pumped by the third harmonic of the Nd:YAG laser. The 34 ns time delay is to avoid temporal and spatial overlap between the IR laser and dye laser pulses. IR and dye lasers are combined and focused by the 175 mm convex lens. The dye laser divergence is controlled by a set of convex lenses in order to compensate for chromatic aberration and to locate IR and dye foci at the same *x* coordinate. A 0.15 mJ dye laser pulse ionizes the molecules mostly into molecular ions by the REMPI process, $^1E_{1u}\leftarrow{}^1B_{2u}\leftarrow\tilde{X}\,{}^1A_{1g}(2+1+1)$ for benzene[14] and $[^2\Pi_{g3/2}]4p\sigma_u,(^3\Pi_u)\leftarrow\tilde{X}\,{}^1\Sigma_g^+(3+1)$ for CS_2.[15]

The deflected and subsequently ionized molecules fly into a 570 mm TOF tube along the molecular beam axis (*z* axis) guided by an electrostatic lens system of three electrode plates: a repeller, an extractor, and a ground (Fig. 1). These electrodes are made of 2-mm-thick aluminum and have an outer diameter of 110 mm. The distances from the repeller to the extractor and from the extractor to the ground are 35 mm and 15 mm, respectively. The repeller and extractor electrodes have a central part made of stainless steel. The 0.6 mm diam pinhole at the center of the repeller determines the molecular beam size. There is a 10 mm diam hole at the stainless steel center of the extractor instead of the grids usually used in molecular fragmentation experiments.[11] The repeller voltage is varied from 150 V to 1500 V and the extractor voltage from 100 V to 1000 V keeping the ion focusing condition. The ground electrode has a hatlike shape with a 1 mm thick and 20 mm long head, which minimizes distortion of the electric field.

When the ion image is focused on a 2D detector using a combination of the three electrodes without grids, ions of the same velocity are mapped onto the same position regardless of their initial positions. If molecular ions with $v_y=0$ are focused onto one point ($Y=0$) at the detector, the ions having a velocity of v_y are focused on the point $Y=v_y\times$TOF. Therefore, although the trajectories of molecular ions differ from those of neutral molecules, the shifts due to the velocity v_y ($\Delta Y=v_y\times$TOF) are retained regardless of the electric field of the electrodes. This focusing electrode configuration is called velocity map imaging.[11] Since blurring due to a finite ionization volume and distortions in the ionic trajectory induced by grid wires are removed and all the ions are transmitted in this scheme, the signal intensity and resolution of images focused by the gridless electrostatic lens system are dramatically enhanced. The focal length of the electrostatic lens is controlled by varying the ratio of the extractor voltage

V_E to the repeller voltage V_R. For our electrode system, a ratio of 2:3 gives optimal focusing at the 2D detector located 680 mm from the ionizing region.

After passing through the ground electrode, ions fly to a 40 mm diam chevron-type microchannel plate (MCP; 3040-FM, Galileo) with a constant velocity determined by the electrode voltages. Signal amplification of MCP is highly nonlinear in the voltage difference across the front and back of the MCP. Up to 1300 V, no output signals are observed and a voltage of 1800 V is used for detection. To detect molecular ions only, the MCP is gated by a negative high voltage pulse. A voltage of 1300 V is constantly applied to the back side of the MCP using a high voltage power supply. A -500 V pulse generated by a homemade pulse generator using another high voltage power supply and a delay generator (DG535, Stanford Research Systems) is applied to the front side when the molecular ions reach the MCP. Electrons emerging from the back of the MCP impinge on a P47 phosphor screen (Galileo) which is activated by applying a voltage of 3600 V.

The 2D emissions from the phosphor screen are intensified about 100 times by an image intensifier (Quantum leap 5n, Stanford Computer Optics) and recorded by a charge coupled device (CCD) camera (512×512 pixels, CH350/L, Photometrics). The same triggering TTL pulse used for gating the MCP activates the image intensifier. The noise near time zero generated by lasers is removed and the background level is lowered by about 5%. Although the intensified images of molecular ions from ten laser shots are sufficiently clear, three sets of 600-shot ion images are integrated by the CCD camera in order to reduce the effects from drifts and fluctuations in laser intensities and ion optics voltages. By averaging 1800 shots, a more than 40-fold reduction ($\approx\sqrt{1800}$) in fluctuations is obtained.

The CCD camera and other instruments are controlled using internal scripts implemented in the V++ software (Photometrics). The ion images are stored as unsigned 16-bit words. The maximum signal intensity of a pixel of a 600-shot image ranges from 3 000 to 30 000 as the V_R is varied from 150 V to 1500 V. Noise per pixel for a 600-shot image is about 10 and is reduced by half when the background image obtained without the molecular beam is subtracted.

In order to investigate the effects of the IR laser pulse on the molecular beam, ion images on the CCD detector with and without the IR laser beam are compared. A computer-controlled homemade shutter is used to block the IR laser. The CCD signals of 40 pixels along the x axis near the x center of the image are binned together to obtain the profiles. The basic parameters of the deflecting laser fields such as the waist radius (ω_0) and the potential well depth (U_0) are determined by scanning the dye laser position along the y axis near the IR laser center and comparing the deflection results with the theoretical ones.

Emissions from the phosphor screen are also monitored by a photomultiplier tube (PMT; 1P21/E717-21, Hamamatsu), and displayed on a digital storage oscilloscope (Infinium 54845A, Agilent). This dual detection method is useful for optical alignment, MCP time gating, and ray tracing in which it is necessary to measure both the image shift and the TOF. Since the rise time of MCP and PMT are 550 ps and 2.2 ns, respectively, the overall response mostly depends on the P47 phosphor screen having a 100-ns decay time to 10% of the maximum intensity. In the experiment, the resolution (R = TOF/2FWHM) of our system is about 100 when the repeller and extractor voltages are 1500 V and 1000 V, respectively.

Owing to the drastically improved resolution of the velocity map imaging technique, tracing of the molecular rays affected by a cylindrical molecular lens can be achieved by measuring ΔY and the TOF of molecular ions. Molecular ions created by the REMPI processes are accelerated by the electrode system and then fly to the MCP with a constant velocity. During the traveling time of molecular ions (=TOF), unaccelerated neutral molecules would proceed a distance of TOF$\times v_z$ (neutral molecule) along the z axis with the same y-shift as molecular ions (ΔY). Note that the velocity changes during the chosen REMPI processes are negligible and the velocity of a molecular ion is the same as that of the parent neutral molecule; v_y(neutral molecule) $\approx v_y$(molecular ion). Thus the trajectories of neutral molecules $(y_0;x=0,y,z)$ passing through the lens at $y=y_0$, where the origin (0, 0, 0) represents the center of the IR laser focus are given by

$$y=y_0+\Delta Y, \quad z=v_z\times\mathrm{TOF}. \tag{2}$$

By varying the electrode voltages while keeping the ratio V_E/V_R constant for ion focusing, the distance to the detector is scaled in proportion to the TOF of molecular ions; the distance to the detector plane is virtually changed. Therefore, ray tracing of the molecular lens can be achieved by measuring ΔY and the TOF at each y_0 value as the electrode voltages are varied. ΔY is measured by comparing ion images for undeflected and deflected molecules, and a TOF value is obtained from the PMT signals. The extrapolations of the regression lines for the trajectories $(y_0;0,y,z)$ of neutral molecules at several y_0 values yield the characteristic parameters of the molecular lens.

III. THEORY

A. Deflection of molecules by the induced dipole force

In the presence of a static electric field **E**, molecules are located in the potential well due to the Stark shift[16]

$$U=-\tfrac{1}{2}\alpha|\mathbf{E}|^2. \tag{3}$$

For a time-varying electric field the Stark shift is given by

$$U(x,y,z,t)=-\tfrac{1}{4}\alpha E(x,y,z,t)^2, \tag{4}$$

where α is the static molecular polarizability and $E(x,y,z,t)$ is the space- and time-dependent electric field envelope. For a laser pulse with a Gaussian intensity profile at $x=0$ propagating along the x axis,

$$I=I_0\exp[-2(y^2+z^2)/\omega_0^2]\exp[-4\ln 2(t^2/\tau^2)], \tag{5}$$

and the induced dipole force along the y axis, F_y, is given by

$$F_y = -\nabla_y U$$
$$= -4\frac{U_0}{\omega_0^2} y \exp\left\{-\frac{2[(v_z t)^2 + y^2]}{\omega_0^2}\right\} \exp\left\{-4\ln 2\left(\frac{t^2}{\tau^2}\right)\right\}, \tag{6}$$

where t is time, τ is the FWHM of a laser pulse, $z = v_z t$ is the z coordinate of the molecules, and U_0 is the maximum Stark shift at the laser pulse peak,

$$U_0 = -\tfrac{1}{4}\alpha E_0^2 = -\tfrac{1}{2}\alpha \eta_0 I_0 \tag{7}$$

with the impedance of vacuum η_0 and the laser peak intensity I_0. The effect of the z component of the induced dipole force can be neglected for the case $v_z \gg \Delta v_z$. It is also possible to neglect changes in the molecule's y coordinate during the deflection when $\Delta v_y \tau \ll y$. The experimentally observed velocity shift is then given by[2]

$$\Delta v_y = \frac{1}{m}\int_{-\infty}^{\infty} F_y(t)\,dt, \tag{8}$$

yielding

$$\Delta v_y = \frac{\Delta Y}{\mathrm{TOF}} = -\frac{2\sqrt{2\pi} U_0 y \exp(-2y^2/\omega_0^2)}{m\omega_0 v_z \sqrt{1 + 2\ln 2(\omega_0/[v_z\tau])^2}}, \tag{9}$$

where m is the mass of a molecule. This implies that the molecular velocity change due to the IR laser depends on m, α, and I_0 as follows:

$$\Delta v_y \propto \frac{U_0}{m} \propto \frac{\alpha I_0}{m}. \tag{10}$$

$|\Delta v_y|$ reaches a maximum at $y = \pm\omega_0/2$. The sign of Δv_y is negative if $y > 0$ and vice versa. This deflection effect results in the focusing of a molecular beam as an optical lens focuses a light beam. As in the case of an optical lens, we can define and determine the associated lens parameters.

B. Molecular ray tracing

By assuming, for convenience, a virtual aperture blocking the molecular beam with $|y_0| > \omega_0$ as in Fig. 2, the characteristic parameters of a molecular lens can be obtained from the traces of molecular rays. The focal length, f, is defined as the distance to the point of maximum molecular density. W is the minimum molecular beam width in the y direction and D is the z value at which the molecular beam width is W.

To determine f, let us consider a group of N_0 molecules in the yz plane passing through a cylindrical molecular lens of aperture width, $2\omega_0$. At $t = 0$, the molecules are equally distributed along the y axis and all the molecules have the same initial velocities, $\mathbf{v}(0) = v_z(0)\hat{z}$. As molecules pass by the molecular lens, v_z increases before the IR focus center and then decreases after the center. Since these two effects mostly cancel each other out, the effects of the molecular lens on v_z can be effectively accounted for by assuming the same initial velocities along the aperture and neglecting the changes in v_z. Let $\lambda(y,z)$ be the line density function:

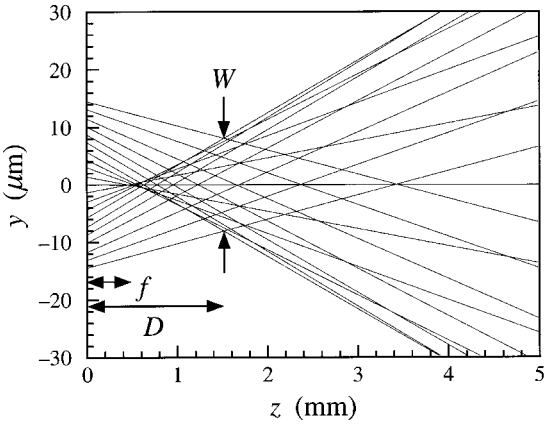

FIG. 2. Theoretical trajectories of benzene molecular rays within $\pm\omega_0$ exerted by a molecular lens are shown. The peak intensity of the laser (I_0) is 5.3×10^{11} W/cm^2 and the waist radius (ω_0) is 14.5 μm. The lens parameters are indicated: W is the minimum beam width, D the distance to the minimum beam width position, and f is the focal length of the molecular lens.

$\lambda(y,z)dy$ is the number of molecules in dy along the line $z = v_z t$ at position (y, z). At $z = 0$, the molecular distribution is constant over the aperture,

$$\lambda(y,0) = \frac{N_0}{2\omega_0} = \lambda_0. \tag{11}$$

From Eq. (2), the trajectory of a molecule passing through the lens at y_0 is given by the line,

$$y = y_0 + \frac{\Delta v_y(y_0)}{v_z} z. \tag{12}$$

After a little algebra,[17] the focal length f, the z coordinate at which $\lambda(y,z)$ is maximum, is given by

$$f = \frac{a}{I_0}, \tag{13}$$

where

$$a = \frac{m\omega_0 v_z^2 \sqrt{1 + 2\ln 2[\omega_0/(v_z\tau)]^2}}{\sqrt{2\pi}\alpha\eta_0}. \tag{14}$$

W is determined by the intersection of two rays starting from $y_0 = +\omega_0(-\omega_0)$ and $y_0 = -\beta\omega_0(+\beta\omega_0)$ $(0 \leqslant \beta \leqslant 1)$. From Eqs. (9) and (12), the y value of the intersection y_{int} is given by

$$y_{\mathrm{int}}(\beta) = -\omega_0 + \omega_0 \frac{(1+\beta)e^{-2}}{\beta e^{-2\beta^2} + e^{-2}}. \tag{15}$$

From the condition $\partial y_{\mathrm{int}}/\partial\beta = 0$, the minimum y_{int} is obtained with $\beta = 0.384$. Then W and D are given by

$$W = 1.1\ \ \omega_0, \tag{16}$$

$$D = 3.3\frac{a}{I_0}. \tag{17}$$

The intensity dependence of the lens parameters is obvious. While W is independent of the laser intensity, D and f are proportional to the inverse of laser intensity $(1/I_0)$ according

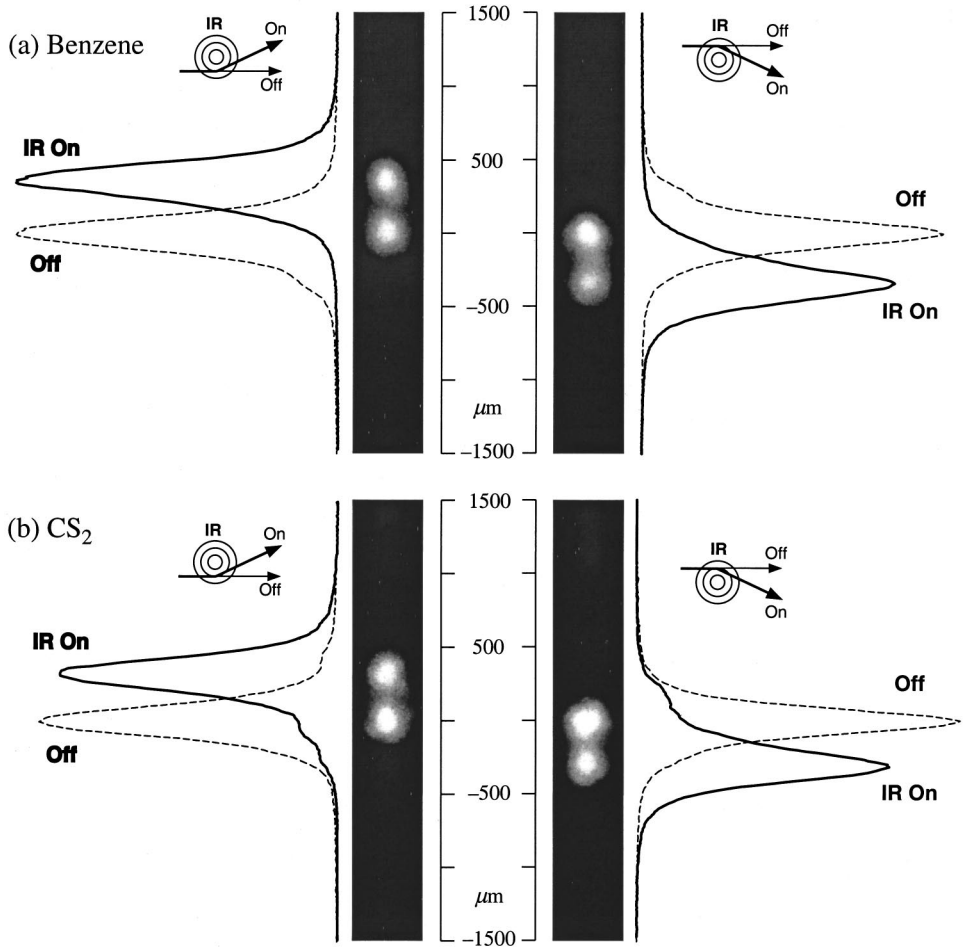

FIG. 3. Portion of the velocity-mapped ion images of deflected molecules and their profiles at the detector of the undeflected (Off) molecules and the deflected molecules (IR On). Schemes show the relative locations of the foci of the IR laser and the dye laser. The velocity change due to the molecular lens can be estimated from the image shift. The vertical scale shows the distance along the y axis on the phosphor screen. The IR laser is circularly polarized and of peak intensity (a) $I_0 = 8.4 \times 10^{11}$ W/cm^2 for benzene, and (b) $I_0 = 8.1 \times 10^{11}$ W/cm^2 for CS_2.

to Eqs. (13) and (17), and the ratio of their slopes is 3.3. In addition, since a is proportional to m/α, D and f are proportional to m/α, while W is independent of it.

IV. RESULTS AND DISCUSSION

A. Deflection of molecules

Shown in Fig. 3 are ion images of the molecular beams of benzene and CS_2 deflected by the IR Nd:YAG laser pulses with reference images of the undeflected molecular beams. The peak intensity I_0 of the laser pulse for deflecting benzene is 8.4×10^{11} W/cm^2. The benzene molecular ion image with 0.24-mm FWHM obtained by focusing the ionizing dye laser beam 7.6 μm above (below) the IR laser focus is shifted 0.35 mm downward (upward). These image shifts and a 42-μs TOF with a repeller voltage of 150 V correspond to $\Delta v_y = \pm 8.3$ m/s. The chromatographic resolution (Rs) (Ref. 18) between the undeflected and the deflected images is given by $Rs \equiv 0.589\ \Delta y_{\text{peak}}/W_{1/2} = 0.84$, where Δy_{peak} and $W_{1/2}$ are the distance between the peaks and the FWHMs of the two images, respectively. The resolution of the CS_2 ion image is 0.80 at the same laser intensity of 8.1×10^{11} W/cm^2.

The velocity spread (FWHM) of 4.8 m/s for CS_2 and 5.4 m/s for benzene estimated from the ion images of undeflected molecular rays should be a convolution of several factors including the initial transverse velocity spread ($\Delta v_{\text{trans}}^{\text{init}}$) of the molecular beam, velocity changes during ionization, and blurring at the detector.

Molecular beam geometry determines the initial transverse velocity spread. Simple line-of-sight arguments give $\Delta v_{\text{trans}}^{\text{init}}$ as

$$\Delta v_{\text{trans}}^{\text{init}} = \frac{D_N}{l/v_z}, \tag{18}$$

where D_N is the nozzle diameter and l the distance from the nozzle to the dye laser focus.[2] Substituting the values of $D_N = 0.5$ mm and $l = 85$ mm, $\Delta v_{\text{trans}}^{\text{init}} = 3.4$ m/s.

The maximum velocity change during the REMPI processes (Δv_{REMPI}) can be estimated from the photoelectron kinetic energy and the momentum conservation law. The photoelectron energies of benzene and CS_2 are 1.15 eV and 0.18 eV, which give transverse velocities of 4.5 m/s and 1.8 m/s, respectively.[14,15] Benzene undergoes a vibrational relaxation[14] with a rate[19] of 10^{14} s^{-1} after reaching high vibrational levels of the $^1E_{1u}$ electronic state by absorbing the third photon with a wavelength of 477.4 nm. The ionization rate from the $^1E_{1u}$ state is estimated to be 10^{12} s^{-1} for a dye laser intensity of 2×10^{10} W/cm^2.[14] Therefore, the vibrational relaxation should be a much faster process than the ionization. As much as 0.82 eV of energy is lost during the relaxation process[14] and the photoelectron energy is lowered

to 0.33 eV which results in a reduction of the transverse velocity spread of benzene molecular ions from 4.5 m/s to 2.4 m/s.

The charge clouds of the amplified electrons ejected from the MCP give rise to a blurring in the phosphor screen image.[20,21] The smallest images of ions produced by ten laser shots of minimal dye laser intensity has a spread of 130 μm FWHM which corresponds to a velocity spread ($\Delta v_{\text{detector}}$) of 3.1 m/s under the present experimental conditions. Therefore, it is estimated that 130 μm is the minimum image size. Note that the smallest detectable change in the center of an image could be much smaller than the minimum image size. Assuming that these contributions are random and independent, the total velocity spread $\Delta v_{\text{tot}} \approx \sqrt{(\Delta v_{\text{trans}}^{\text{init}})^2+(\Delta v_{\text{REMPI}})^2+(\Delta v_{\text{detector}})^2}$, which gives 5.2 m/s for benzene and 4.9 m/s for CS_2. These values agree well with those from the image size: 5.4 m/s and 4.8 m/s, respectively.

The deflected images are about 10% larger than the undeflected ones. This extra spread comes from the finite pulse duration and size of the ionizing laser. For a given time delay (=34 ns) between the deflecting and ionizing laser pulses, the spatial delay between the deflecting laser pulse and the ionizing laser pulse is adjusted to achieve the maximum deflection; the molecules passing $z=0$ at $t=0$ also pass the center of the ionization region when the intensity of the ionizing laser is at its peak. Due to the finite size ($\omega_0 = 10\,\mu$m) and pulse duration ($\tau=5$ ns) of the ionizing laser, molecules which have been near $z=0$ at $t=0$ are also ionized. In a four-photon REMPI process, the ionization probability profile will be proportional to I^4 and be a Gaussian with $\omega_0 \approx 5\,\mu$m and $\tau=2.5$ ns. These effects cause the deflection near the maximum points ($y=\pm\omega_0/2$) to be underestimated since the velocities spread to the lower values. At most other points the velocities spread to higher and lower values. We estimate the overall broadening due to these effects to be up to about 1.5 m/s corresponding to a 6% increase in the image size when convoluted with other broadening effects. A typical longitudinal velocity spread of a supersonic beam is less than 10% (FWHM) of its average velocity.[22] This velocity spread will result in about 10% spreads of f and D values. However, the influence of this spread in v_z is negligible in measuring Δv_y from ion images. Ions are accelerated to have velocities 20 times larger than the neutral beam velocity and the angular spread of ions of the deflected molecular beam due to the 10% spread in v_z is less than 0.5% of its deflection angle.

Deflection of the molecular beam as a function of y is obtained by changing the y position of the dye laser focus. Figure 4 shows Δv_y of the molecules with a 44 mJ circularly polarized IR pulse. With a V_R of 150 V, TOFs for molecular ions are 42 μs. Using the molecular beam speed $v_z = 570$ m/s for benzene and 560 m/s for CS_2 at 293 K calculated from Eq. (1), and an IR pulse of $I_0 = 5.8\times10^{11}$ W/cm^2 with duration $\tau=7$ ns, the experimental data are excellently fitted by Eq. (9) as shown by the solid lines in Fig. 4. The fit for benzene yields an IR laser waist radius (ω_0) 14.5 μm and potential well depths (U_0) of 7.9 meV [Fig. 4(a)]. For CS_2,

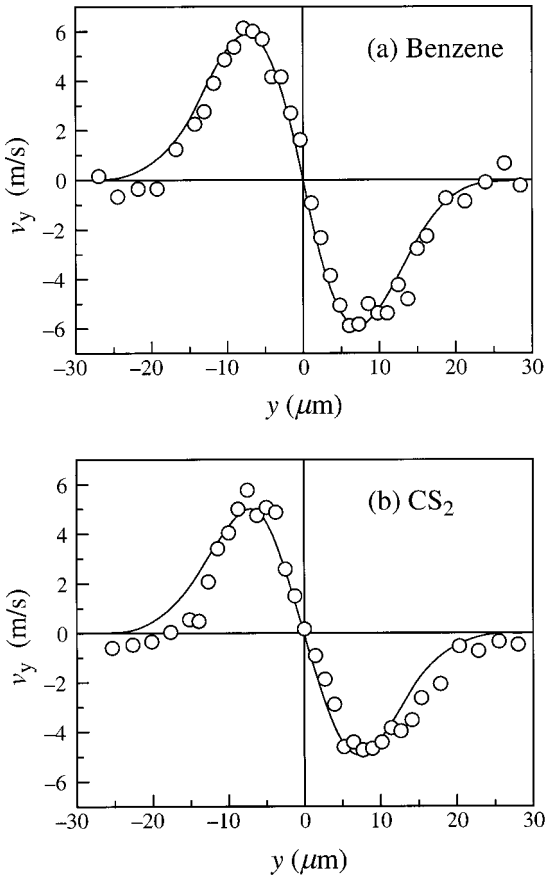

FIG. 4. The deflection velocity changes along the y axis are plotted as a function of the relative positions of the IR laser focus from the dye laser focus. The IR laser is circularly polarized with peak intensity $I_0 = 5.8\times10^{11}$ W/cm^2. The solid curves show the fitting results from which ω_0 and U_0 are calculated using Eq. (11). (a) Benzene, $\omega_0 = 14.5\,\mu$m and $U_0 = 7.9$ meV. (b) CS_2, $\omega_0 = 14.2\,\mu$m and $U_0 = 6.3$ meV.

the values obtained from the fit are $\omega_0 = 14.2\,\mu$m and $U_0 = 6.3$ meV [Fig. 4(b)].

Using a pulse energy of 44 mJ and an average static polarizability[23] $\alpha = 11.6\times10^{-40}$ C m^2/V for benzene and $\alpha = 9.6\times10^{-40}$ C m^2/V for CS_2, Eq. (7) yields values of $U_0 = 24$ meV and 21 meV for benzene and CS_2, respectively. The differences between the two sets of U_0 values estimated from Eq. (7) and Eq. (9) are due to the complicated spatial beam mode of the IR pulse and uncertainties in measuring the waist radii. The Nd:YAG laser generates pulses at a fundamental wavelength of 1064 nm. To pump the dye laser, the third harmonic at 355 nm are obtained by passing the fundamental beam through the second and the third harmonic generation crystals. The remaining fundamental component is then used to deflect the molecular beam. We obtain the intensity profile of the focused laser by scanning with a 12.5 μm diam aperture in the vicinity of the waist of the residual fundamental beam focused with the 175-mm-focal-length convex lens. There are three peaks along the y axis and the deconvolution of the central peak gives $\omega_0 = 16.3\,\mu$m. Since only the major peak is used for the scanning studies, the peak intensity calculated from the total energy of the beam is certainly overestimated. Moreover, an error of only 1 μm in measuring ω_0 for the IR laser leads to an 11% error in the

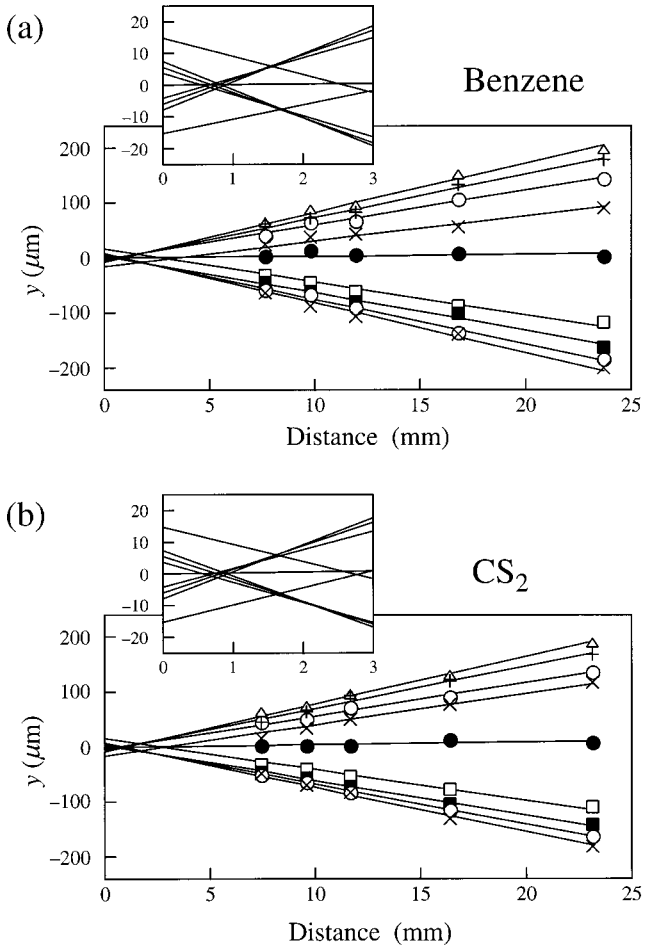

FIG. 5. Tracing of molecular rays passing through the cylindrical lens of width $2\omega_0$ formed by the IR laser. The IR laser is circularly polarized with peak intensity $I_0=5.3\times10^{11}$ W/cm^2. The insert box shows the region near the molecular lens focus. The result (a) is for benzene and (b) is for CS_2. Each set of data with the same symbol represents the trajectory of molecules starting from the same point, and each trajectory is obtained by least-squares fit. Horizontal scale is the distance from the lens traveled by neutral molecules during the TOF given by the product v_z(neutral molecule) $\times$TOF(moleular ion).

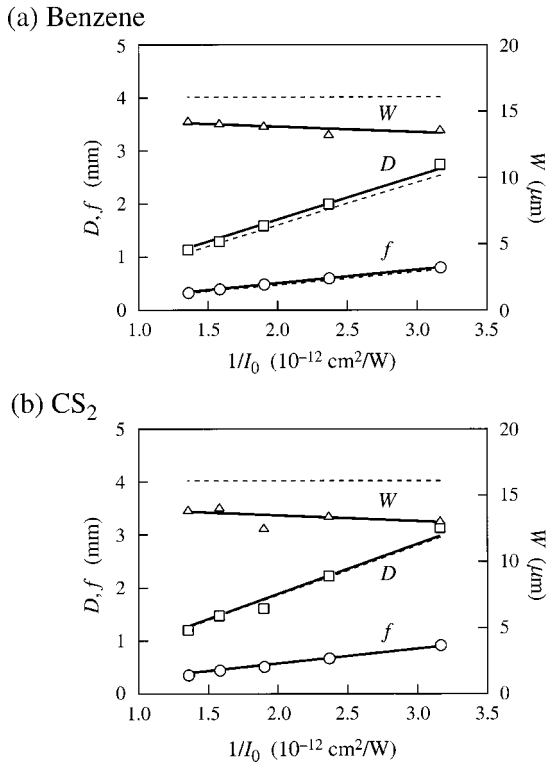

FIG. 6. Intensity dependence of the characteristic parameters of the molecular lens. W is the minimum beam width, D the distance to the minimum beam width position, and f is the focal length of the lens. Solid lines are fits of the experimental results and dotted lines are the theoretical predictions for (a) benzene and (b) CS_2. W is independent of the peak intensity of the IR laser, while D and f are proportional to the inverse of the peak intensity. D and f are inversely proportional to the polarizability per mass of a molecule α/m and W is insensitive to the molecular species.

peak intensity. Therefore, the peak intensity calculated from the laser pulse energy by Eq. (7) requires calibration. As the deflecting laser intensity is varied, the ratios of the two U_0 values estimated from Eq. (7) and Eq. (9) remain constant at 3.1, the value which is used as an intensity calibration factor. In addition, the ratio $U_0(\text{benzene})/U_0(CS_2)=1.2$ agrees with the theoretical ratio $(\alpha/m)(\text{benzene})/(\alpha/m)(CS_2)=1.2$, supporting the intensity calibration method used in this work.

B. Tracing of the molecular beams

Molecular rays passing through the cylindrical molecular lens of width $2\omega_0$ are traced by placing the ionizing dye laser focus at representative points, $y_0=0$, $\pm0.25\omega_0$, $\pm0.384\omega_0$, $\pm0.50\omega_0$, $\pm\omega_0$. Figure 5 shows the experimentally obtained trajectories in the yz plane. The peak laser intensity forming this cylindrical lens is 5.3×10^{11} W/cm^2. W and D are obtained from the intersection of molecular rays starting at ω_0 $(-\omega_0)$ and -0.384 ω_0 $(0.384\,\omega_0)$. For experimental convenience, we measure the distance $f'[=(a/I_0)e^{1/2}]$ to the intersecting point of the two most deflected molecular rays, which pass the molecular lens at $\omega_0/2$ and $-\omega_0/2$, and calculate f from the relation $f=f'/e^{1/2}$.

The experimentally obtained values of D, W, and f are shown in Fig. 6 as a function of $1/I_0$. The energy per IR laser pulse is varied from 24 mJ to 56 mJ. As discussed above, the peak intensity is corrected using the calibration factor of 3.1. W is independent of the peak intensity, whereas f and D are proportional to $1/I_0$. In addition, the ratio between the slopes for D and f is 3.3. In Table I, experimental and theoretical values of the molecular lens parameters are compared. These are in excellent agreement with Eqs. (13), (16), and (17) (dashed lines).

In the previous theoretical work, the focal length was expressed as $f/\omega_0'=\sqrt{R}/\sin(2/\sqrt{R})$, where R is the ratio of

TABLE I. Experimental and theoretical values of the molecular lens parameters.

	Benzene	CS_2	Theoretical
f	$1.1\,a/I_0$	$1.0\,a/I_0$	$1.0\,a/I_0$
D	$3.5\,a/I_0$	$3.4\,a/I_0$	$3.3\,a/I_0$
W	$0.96\,\omega_0$	$0.93\,\omega_0$	$1.1\,\omega_0$

TABLE II. Ratios of various lens parameters for CS_2 and benzene.

	Experiment	Theory
$U_0^{-1}(CS_2)/U_0^{-1}$(benzene)	1.2	1.2
$f(CS_2)/f$(benzene)	1.1	1.2
$D(CS_2)/D$(benzene)	1.1	1.2
$W(CS_2)/W$(benzene)	0.97	1.0

the kinetic energy of a molecule to the potential energy depth by light-molecule interaction.[8] (Note that ω_0' in Ref. 8 is $1/\sqrt{2}$ of the waist radius, ω_0, in this paper.) The kinetic energies of benzene and CS_2 molecules can be calculated easily from their beam velocities, 570 m/s for benzene and 560 m/s for CS_2. At a laser intensity of 5.8×10^{11} W/cm^2, the potential well depths are 7.9 meV and 6.3 meV, respectively. In Ref. 8, the potential well depth is treated as a time-independent quantity when molecules pass the laser. In our case, however, the time taken by the molecules to traverse the distance $2\omega_0'(=21\ \mu\text{m})$ is about 36 ns, which is longer than the laser pulse duration of 7 ns (FWHM). Therefore, the potential well depth is a time-dependent function and should be averaged over time to traverse $2\omega_0'$ for comparison. Then the theoretical focal lengths (f/ω_0') are 40 for benzene and 48 for CS_2 and the experimental values for benzene and CS_2 are 43 and 48, respectively. They indicate good agreement between previous theoretical work and our current work.

The dependence of the lens parameters on the polarizability per mass α/m also agrees well with the prediction (see Table II). Since the parameter a is inversely proportional to α/m, D and f are inversely proportional to α/m, while W is independent of α/m. Both the ratios $D(CS_2)/D$(benzene) and $f(CS_2)/f$(benzene) are 1.1. These values are nearly equal to the polarizability per mass ratio α/m(benzene)/$\alpha/m(CS_2)$ of 1.2. On the other hand, the ratio $W(CS_2)/W$(benzene) is 0.97, independent of α/m.

C. Aperture size dependence of the lens parameters

As noted in the previous subsection, the ratio of D to f was 3.2 and 3.4 for benzene and CS_2, respectively. This represents the lens aberration due to the aperture size. The closer to 1 the ratio is, the smaller is the aberration. Since the linear region of the deflection velocity is $|y|<\omega_0/2$ as shown in Fig. 4, the aperture size should be reduced to at least ω_0 to reduce the lens aberration. Let the aperture size be $2w_a$. Then D and W can be found easily from the intersection points of the lines starting from $y_0=+w_a(-w_a)$ and $y_0=-\beta w_a(+\beta w_a)$. The y value of the intersection y_{int} is then given by

$$y_{\text{int}}(\beta)=-w_a+w_a\frac{(1+\beta)e^{-2(w_a/\omega_0)^2}}{\beta e^{-2\beta^2(w_a/\omega_0)^2}+e^{-2(w_a/\omega_0)^2}}. \quad (19)$$

The lens parameters obtained by minimizing $y_{\text{int}}(\beta)$ are shown in Fig. 7. f is independent of the aperture size since the maximum density point is determined by the molecular ray starting from near $y_0=0$ and is not influenced by the aperture size. D and W decrease rapidly as the aperture size is reduced. When the aperture size $2w_a=0.5\omega_0$, $D=1.1a/I_0$ and $W=0.016\omega_0$, and the lens aberration is negligible. ($D/f=1.1$ and W is 3.2% of the initial width, $2w_a$.)

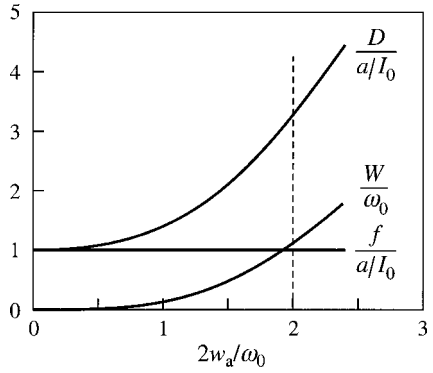

FIG. 7. Variations of the lens parameters according to the aperture size ($2w_a$). As the aperture size gets close to 0, D approaches f and W approaches 0, which means the lens aberration becomes small. The dotted line represents the molecular lens in this report ($2w_a=2\omega_0$).

D. Laser polarization effects

Since the polarizability of a symmetric top molecule is anisotropic, the potential well depth felt by the molecule depends on the angle θ between the molecular axis and the laser polarization. The Stark shift is given by

$$U=-\tfrac{1}{4}\alpha_{\text{eff}}E^2=-\tfrac{1}{4}[(\alpha_\parallel-\alpha_\perp)\cos^2\theta+\alpha_\perp]E^2, \quad (20)$$

where α_{eff} is the effective polarizability and $\alpha_\parallel$ and $\alpha_\perp$ are the polarizability components parallel and perpendicular to the molecular axis, respectively.[24] Since molecules seek an angle of low potential energy, they will be aligned with the laser polarization direction. Therefore, the molecules have different $\langle\cos^2\theta\rangle$ values depending on the degree of alignment; $\langle\cos^2\theta\rangle=1$ for perfectly aligned molecules and 1/3 for randomly oriented molecules. Several theoretical predictions[3,25–27] and experimental results[4–6] have been reported on the alignment of molecules in laser fields. In general, the average value $\langle\cos^2\theta\rangle$ depends on the laser intensity; the increase in the laser intensity causes $\langle\cos^2\theta\rangle$ to be closer to 1.

When the alignment effect is absent, the rotationally averaged polarizability of a symmetric top molecule is the same for both the cases of linear polarization and circular polarization as $\alpha_{\text{ave}}=(\alpha_\parallel+2\alpha_\perp)/3$. If molecules are perfectly aligned with the laser polarization direction, the molecular polarizability depends on the laser polarization and the molecular shape. For linear molecules such as CS_2, $\alpha_\parallel$ ($=16.8\times10^{-40}$ C m^2/V) is larger than $\alpha_\perp$ ($=6.2\times10^{-40}$ C m^2/V).[28] The effective polarizability will not be α_{ave} but $\alpha_\parallel$ if aligned with a linearly polarized field and $(\alpha_\parallel+\alpha_\perp)/2$ ($=11.5\times10^{-40}$ C m^2/V) if aligned with a circularly polarized field. On the other hand, oblate molecules such as benzene have a larger value of $\alpha_\perp$ ($=13.7\times10^{-40}$ C m^2/V) than $\alpha_\parallel$ ($=7.1\times10^{-40}$ C m^2/V), and the effective polarizability is $\alpha_\perp$ for the both polarization cases.

In this study, however, the results do not show an alignment effect. If there is an alignment effect, α_{eff} of Eq. (20) depends on the laser intensity and U is not linear in the laser

intensity. Then, the focal length will not be linear with respect to the inverse of laser intensity. However, the linear dependence of focal length on $1/I_0$ shown in Fig. 6 is evidence against the possibility of molecular alignment. The lack of an alignment effect is probably due to the multilongitudinal mode of an IR laser pulse having picosecond temporal spikes. These rapid spikes prevent molecules from aligning themselves with the polarization direction, since the laser field rising time should be long enough for the molecules to be aligned with the laser polarization.[2,3,5] Hence, the alignment of molecules is neglected in the present study.

E. Separation of molecules

The dependence of molecular lens properties on the value of α/m resembles the dispersion of an optical medium depending on the wavelength and α/m can be called a dispersion factor. Analogous to an optical prism, a mixture of neutral molecules with different α_{ave}/m values can be separated by a molecular lens utilizing the nonresonant dipole force. For example, benzene and nitrogen oxide having α_{ave}/m values of $9.0\times10^{-15}\,\text{C m}^2/\text{V kg}$ and $3.8\times10^{-15}\,\text{C m}^2/\text{V kg}$, respectively, could be separated spatially using a molecular lens. This technique can be called ''optical force chromatography.''

Alignment effects can also be utilized to enhance the separation of molecules. Consider a linear molecule and an oblate molecule of similar α_{ave}/m values mixed with other molecules of different α_{ave}/m values. Since circularly polarized lasers produce much lower ionization than linearly polarized lasers,[29,30] it should be easier to separate out the two molecules from the matrix of other molecules using a molecular lens composed of a circularly polarized laser of high peak intensity. For a linearly polarized laser field, linear molecules are more polarizable than oblate molecules although their rotationally averaged polarizabilities are the same. Thus the two can be further separated from each other using a molecular lens of a linearly polarized laser of lower intensity without causing ionization. This combination could act as a tandem molecular-lens separator.

Recently, an elliptically polarized laser field has been used for aligning molecules three-dimensionally.[7] With an electric field vector of elliptical polarization, $\mathbf{E}=E_a\hat{\mathbf{i}}+iE_b\hat{\mathbf{j}}$, where $E_a^2+E_b^2=E_0^2$ (E_0 is constant; constant laser intensity) and $E_a \geqslant E_b$, the Stark shift of a linear molecule is given by

$$U=\frac{1}{4}(\alpha_{\parallel}E_a^2+\alpha_{\perp}E_b^2)=\frac{1}{4}\,\frac{\alpha_{\parallel}+(1-\epsilon^2)\alpha_{\perp}}{2-\epsilon^2}E_0^2, \qquad (21)$$

where $\epsilon=\sqrt{1-(E_b/E_a)^2}$ is the eccentricity of the ellipse, which is 0 for circular polarization and 1 for linear polarization. As discussed in the previous subsection and noted from Eq. (21), linear molecules are deflected more by a linearly polarized laser field than by a circularly polarized one of the same intensity while the deflection of oblate molecules is independent of the polarization. This implies that the degree of deflection can be adjusted not only by the laser intensity but also by the eccentricity which can be easily controlled by rotating a wave plate. Proper combination of the intensity and eccentricity of the laser polarization will determine the optimum separation conditions in optical force chromatography.

V. CONCLUSION

We have constructed a cylindrical molecular lens consisting of a far-off-resonant nanosecond Nd:YAG laser pulse which acts on a molecular beam as an optical lens does on a light beam. This molecular lens is based on the optical dipole force due to the Stark shift. Molecular beams of benzene and CS_2 are deflected by the molecular lens and the trajectories of the affected neutral molecules are determined from those of molecular ions created by a REMPI process. The velocity map imaging technique dramatically improved the resolution of the deflected ion images. The changes in the transverse velocities of molecular beams were as much as 8.3 m/s and a chromatographic resolution of 0.84 between the deflected and undeflected molecular beams was obtained. Tracing of the trajectories of the deflected molecules allowed us to determine the characteristic parameters of the molecular lens including the focal length, minimum beam width, and distance to the minimum beam width position. The focal length and distance to the minimum beam width position were proportional to the inverse of laser peak intensity and polarizability per mass, whereas the minimum beam width was independent of these quantities. These successful applications of a molecular lens to the molecular beams of benzene and CS_2 confirm the universality of molecular optics. The possibility of separating molecules from a mixture based on their different polarizability per mass values was also investigated as a new type of optical force chromatography.

ACKNOWLEDGMENTS

This work was supported by the CRI and the BK 21 Project in 2001, Korea.

[1] H. Stapelfeldt, H. Sakai, E. Constant, and P. B. Corkum, Phys. Rev. Lett. **79**, 2787 (1997).
[2] H. Sakai, A. Tarasevitch, J. Danilov, H. Stapelfeldt, R. W. Yip, C. Ellert, E. Constant, and P. B. Corkum, Phys. Rev. A **57**, 2794 (1998).
[3] B. Friedrich and D. Herschbach, Phys. Rev. Lett. **74**, 4623 (1995).
[4] W. Kim and P. M. Felker, J. Chem. Phys. **104**, 1147 (1996).
[5] H. Sakai, C. P. Safvan, J. J. Larsen, K. M. Hilligsoe, K. Hald, and H. Stapelfeldt, J. Chem. Phys. **110**, 10235 (1999).
[6] A. Sugita, M. Mashino, M. Kawasaki, Y. Matsumi, R. J. Gordon, and R. Bersohn, J. Chem. Phys. **112**, 2164 (2000).
[7] J. J. Larsen, K. Hald, N. Bjerre, H. Stapelfeldt, and T. Seideman, Phys. Rev. Lett. **85**, 2470 (2000).
[8] T. Seideman, J. Chem. Phys. **106**, 2881 (1997).
[9] T. Seideman, J. Chem. Phys. **107**, 10420 (1997).
[10] B. S. Zhao, H. S. Chung, K. Cho *et al.*, Phys. Rev. Lett. **85**, 2705 (2000).
[11] A. Eppink and D. H. Parker, Rev. Sci. Instrum. **68**, 3477 (1997).
[12] D. R. Miller, in *Atomic and Molecular Beam Methods*, edited by G. Scoles (Oxford University Press, New York, 1988), Vol. 1, p. 17.
[13] P. B. Corkum, N. H. Burnett, and F. Brunel, Phys. Rev. Lett. **62**, 1259 (1989).
[14] Y. Achiba, K. Sato, K. Shobatake, and K. Kimura, J. Chem. Phys. **79**, 5213 (1983).
[15] R. A. Morgan, M. A. Baldwin, A. J. Orr-Ewing, M. N. R. Ashfold, W. J. Buma, J. B. Milan, and C. A. de Lange, J. Chem. Phys. **104**, 6117 (1996).
[16] E. Merzbacher, *Quantum Mechanics*, 2nd ed. (Wiley, New York, 1970).
[17] See EPAPS Document No. E-JCPSA6-114-005120 for the detailed derivation of the focal length *f*. This document may be retrieved via the

EPAPS homepage (http://www.aip.org/pubservs/epaps.html) or from ftp.aip.org in the directory/epaps/. See the EPAPS homepage for more information.
[18] D. C. Harris, *Quantitative Chemical Analysis*, 4th ed. (Freeman, New York, 1995).
[19] B. Katz, M. Brith, B. Sharf, and J. Jortner, J. Chem. Phys. **52**, 88 (1970).
[20] M. L. Edgar, R. Kessel, J. S. Lapington, and D. M. Walton, Rev. Sci. Instrum. **60**, 3673 (1989).
[21] A. S. Tremsin and O. H. W. Siegmund, Rev. Sci. Instrum. **70**, 3282 (1999).
[22] R. B. Bernstein, *Chemical Dynamics via Molecular Beam and Laser Techniques* (Oxford University Press, Oxford, 1982), p. 33.
[23] K. J. Miller, J. Am. Chem. Soc. **112**, 8543 (1990).
[24] J. J. Larsen, H. Sakai, C. P. Safvan, I. Wendt-Larsen, and H. Stapelfeldt, J. Chem. Phys. **111**, 7774 (1999).
[25] C. M. Dion, A. Keller, O. Atabek, and A. D. Bandrauk, Phys. Rev. A **59**, 1382 (1999).
[26] T. Seideman, Phys. Rev. Lett. **83**, 4971 (1999).
[27] A. Keller, C. M. Dion, and O. Atabek, Phys. Rev. A **61**, 023409 (2000).
[28] J. O. Hirschfelder, C. F. Curtiss, and R. B. Bird, *Molecular Theory of Gases and Liquids* (Wiley, New York, 1964).
[29] P. Lambropoulos, in *Advances in Atomic and Molecular Physics*, edited by D. R. Bates and B. Bederson (Academic, New York, 1976), Vol. 12, p. 135.
[30] L. A. Lompre, G. Mainfray, C. Manus, and J. Thebault, Phys. Rev. A **15**, 1604 (1977).